International Journal of Computer Information Systems and Industrial Management Applications
ISSN 2150-7988 Volume 18 (2026) pp. 1-26

https://doi.org/10.70917/ijcisim-2026-0371
Article

Optimization research on automatic control and servo control system of high-precision assembly industrial robot based on variational method

Yan Li [1,*]

[1] Anhui Vocational and Technical College, Hefei, Anhui, 230011, China
* Correspondence author: liyan225588@126.com

Abstract: The development of industrial robotics technology has led to a large number of applications in assembly tasks in production practice, but due to factors such as the complexity of the assembly process, the robot's own positioning accuracy and the limitations of vision technology, there are still great challenges in the control of high-precision assembly of robots. In this paper, a high-precision assembly industrial robot automatic control and servo control system combined with flexible assembly technology is proposed. In this system, an actuation system and a mechanics perception system are designed. The actuation system is based on 6PUS-UPU parallel robots, and the motion control of the assembly robot is realized by kinematic inverse solution. The mechanics sensing system is constructed based on a six-dimensional force sensor as a way to obtain the force/torque data during the assembly process of the industrial robot. Then the robot motion model is linearized using the variational method, and then an ideal impedance model is set for the adjustable parametric impedance control system to realize the supple control of the industrial robot with reference to the adaptive control method. It is found that the optimized automatic control and servo control system of the high-precision assembly industrial robot in this paper has higher assembly efficiency and strong fault-tolerant assembly effect. Therefore, the optimization of the automatic control and servo control system of high-precision assembly industrial robots can lay a solid foundation for improving the industrial production level.

Keywords: industrial robot; variational method; flexible assembly technology; kinematic inverse solution; anti-resistance control strategy

1. Introduction

With the development of science and technology, robotics technology has arisen and developed rapidly, various types of robots in many ways affect people's production and lifestyle, change and improve people's standard of living in a subtle way, and gradually enter the high-tech field, becoming an indispensable part of it [1-3]. In the contemporary era of continuous development and deepening of informationization process, people keep thinking of replacing workers with robots to reduce the degree of work danger and improve the quality of industrial products and work efficiency [4-6]. In the field of manufacturing, the traditional manufacturing industry is being transformed and upgraded to intelligent manufacturing, and industrial robots, as a new type of industrial machinery, can promote the development of the assembly manufacturing industry and provide convenience for the actual production of enterprises [7-10]. The application of industrial robots in the assembly production line largely improves the production efficiency, ensures the production quality, and at the same time reduces

the repetitive work done by human labor before, which plays an indispensable role in the current equipment manufacturing industry [11-13]. Traditional industrial production to intelligent manufacturing production has become a development trend, the research and application of it has great significance to the development of China's industrial science and technology, and at the same time has a wide range of prospects and markets.

In recent years, robot servo control has gradually developed into one of the most active research directions in the field of robotics. Literature [14] designed a vision servo-based control scheme for assembly robots in order to realize the autonomous control of industrial robots in unstructured environments, using vision pipelines to detect action features and issuing velocity commands to control the adjustment of the robot position by means of feature descriptors and machine learning algorithms. Literature [15] places an information-physical fusion-based assembly cell framework into industrial robot production practice, allowing the robot to identify assembly process resources by collecting visual information through sensors and updating the assembly plan in a digital twin to realize a high-precision physical assembly process. Literature [16] analyzes the advantages and shortcomings of the current robot vision servo system, and the combination of machine vision and servo system effectively improves the robot's intelligence and adaptability in dealing with complex tasks, but trajectory planning, multi-sensor combinations, and other aspects still need to be further improved. Literature [17] proposes a warp-network image processing algorithm based on YOLO machine learning algorithm and Version 2 region of interest, which can guide the industrial robot's adaptability and recognition ability of target images in complex environments, and greatly enhances the environmental adaptability of industrial robot vision servo system. Literature [18] discusses the servo control method of the part error in the high-precision assembly process of industrial robots, using the experimental design to obtain the positioning error of different parts and workpieces, and through the calculation of compensation for the initial positional error to make the robot's assembly process performance to achieve the best, the method can effectively shorten the assembly cycle and improve the assembly accuracy. Literature [19] developed an industrial robot motion profile definition method based on the smooth trajectory generation model, through the calculation of the robot joint performance and assembly task requirements, combined with the multivariate optimization method, to generate the best motion path that can balance the assembly accuracy and assembly speed. It is not difficult to find that it is the basic logic of the robot servo control system to allow the industrial robot to acquire the relevant information of the target workpiece in the workspace through sensors or other methods, and thus adjust the robot end position. Therefore, the variational method can be introduced to further enhance the industrial robot's ability to process the information, so that the robot end-effector achieves the desired degree of position, in order to improve its accuracy in performing assembly tasks.

Industrial robots are often used to help replace or assist humans to complete some high-intensity, repetitive manufacturing work, which can liberate humans from heavy labor and greatly promote the development of social productivity. In this paper, a high-precision assembly industrial robot control system combined with flexible assembly technology is proposed, which adopts the variational method to realize the linearization of the motion model of the industrial robot, and then introduces the anti-resistance control to establish the flexible control strategy of the industrial robot. A six-dimensional force sensor is utilized to obtain the motion assembly data of the assembly robot, and the effect of gravity on the sensor data is eliminated by gravity compensation. To ensure the high-precision assembly of industrial robots to provide support, the effectiveness of the control strategy in this paper is verified through simulation, which provides a new research paradigm to improve the application range of high-precision assembly industrial robots and enhance the level of industrial production automation.

2. Key technologies for flexible assembly

In today's industrial field, the development of automation control technology is rapidly changing, which puts forward higher requirements for production efficiency, product quality and production safety. Industrial robot technology, as the key to the automation control field, has been widely used in many industries such as automobile manufacturing, electronics, machining and so on with the advantages of high precision, high speed and high reliability. It can replace manual labor to complete repetitive and dangerous work tasks and realize the automation control of complex production processes. In-depth study of the application of industrial robot technology in the field of automation control is of great practical significance for promoting industrial transformation and upgrading and improving enterprise competitiveness.

2.1. Shaft hole assembly process and state judgment

2.1.1. Analytical modeling of shaft hole assembly process

With the rapid development of industrial robotics technology and the traditional manufacturing industry to the urgent need for intelligent manufacturing transformation and upgrading, industrial robots have become an irreplaceable important equipment and means in the manufacturing industry. Due to the robot's own rigidity, when carrying out precision assembly operations, a small positional deviation will also produce a large contact force, which will lead to the failure of the assembly operation, and may even damage the assembled workpiece as well as the entire assembly system. Among the high-precision assembly tasks, shaft-hole assembly tasks put forward greater requirements for the control performance of industrial robots. Based on this, this paper focuses on the optimization of industrial robot automatic control and servo control system for high-precision shaft hole assembly, in order to enhance the control performance of high-precision shaft hole assembly.

Shaft hole assembly can be divided into two types: non-chamfered shaft hole assembly and chamfered shaft hole assembly according to whether the assembly workpiece is machined with chamfer. Since it is easier to guide the assembly shaft to insert into the hole when there is a chamfer in the assembly hole, it is easier to complete the assembly operation with chamfered shaft hole assembly, and there are three assumptions of quasi-static, rigidity, and friction coefficient equality in the process of shaft hole assembly with supple assembly. The shaft hole assembly process is shown in Fig. 1, which is mainly divided into four stages, i.e., the approach stage, the chamfered contact stage, the insertion adjustment stage, and the assembly completion stage, and the contact state of the shaft holes as well as the force situation are different in each stage [20].

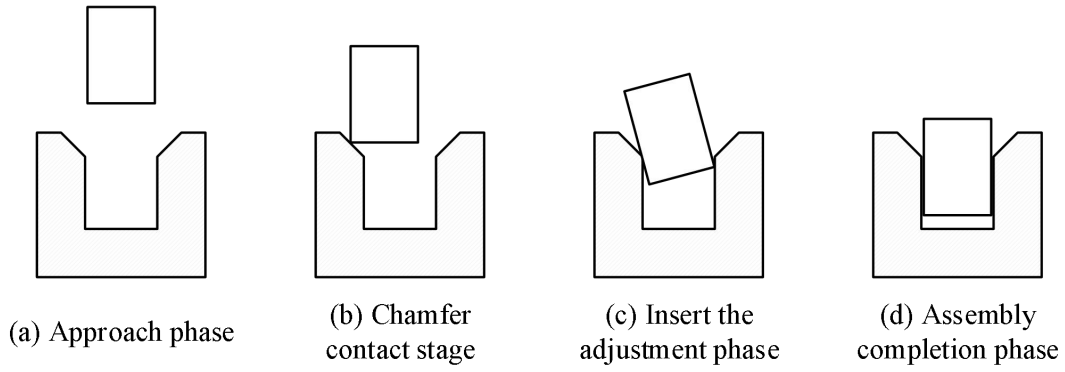

Figure 1. The shaft is assembled at different stages

(1) Approach phase. The robot reaches the assembly axis from the origin through the control system and grasps it, and then transports the assembly axis to the vicinity of the assembly hole for initial positioning, at which time the assembly axis continues to move toward the assembly hole below in accordance with the predetermined trajectory, and the assembly axis does not come into contact with the assembly hole in this process.

(2) Chamfering contact stage. The robot grips the assembly axis and inserts it downward from the top of the assembly hole, and the assembly axis first contacts the chamfered surface of the assembly hole. At this time, certain external environmental constraints are introduced to the robot end gripper, and the robot is converted from the positional localization control at the approach stage to passive suppleness control, and the passive suppleness joints begin to play a major role.

(3) Insertion adjustment and completion of the assembly stage. When the assembly axis is in contact with the chamfer of the assembly hole, the passive supple joint submits to the external environment through the elastic deformation of the spring, so as to make small adjustments to the position of the robot end, realize the automatic compensation of the deviation of the position between the assembly axis and the assembly hole, and make the assembly axis and the center axis of the assembly hole align, so as to complete the assembly of the axis and the hole.

2.1.2. Assembly process contact state judgment

For the high-precision assembly of industrial robot supple mechanism, the premise that can realize the insertion of the shaft into the hole is the contact when the lower end of the shaft falls within the chamfer, which can be obtained as one of the constraints of the assembly feasible domain:

$$u_0 - l_p \sin\theta_0 < R - r + w \tag{1}$$

At the same time, it is necessary to ensure that at the end of the one-point contact phase, the other

end inserted into the bottom face of the shaft is able to slide into the hole without falling above the chamfer on the other side, hence another constraint:

$$2r\cos\theta+(l-l_1)\sin\theta<2R \tag{2}$$

(1) Chamfering contact stage

The force of the manipulator on the workpiece can be expressed as $F=[F_x,F_y,M]$, the contact force as N, and the friction force as f.

Assuming that in the current contact state, the angular error is θ, the offset error is u, and the insertion depth from the beginning of the contact is l, the physical equations and force equations can be established, supplemented with geometric relationship equations based on the positional error, as follows:

The physical relationship is:

$$\begin{cases} f=\mu N \\ F_x=k_x(u_0-u) \\ M=-k_s(\theta_0-\theta) \end{cases} \tag{3}$$

The force relationship is:

$$\begin{cases} F_x=N\sin\alpha-f\cos\alpha \\ F_z=N\cos\alpha+f\sin\alpha \\ M=F_xL_p-F_zr \end{cases} \tag{4}$$

Geometric relations for:

$$u-L_r\sin\theta=u_0-L_p\sin\theta_0-\frac{l}{\tan\alpha} \tag{5}$$

By combining the above equations, the expression for the force on the workpiece can be found as:

$$\begin{bmatrix} F_x \\ F_y \\ M \end{bmatrix}=\begin{bmatrix} F_x \\ AF_x \\ F_xL_p-F_zr \end{bmatrix} \tag{6}$$

Clearly, the insertion depth l has a range of values, viz:

$$0<l<u_0-l_p\sin\theta_0+r-R \tag{7}$$

So far, the relationship between the reaction force $F=[F_x,F_y,M]$ applied to the flexure mechanism and the parameters of the mechanism is established as:

$$F=f(k_x,k_0,u_0,\theta_0,L) \tag{8}$$

Taking this section as an example, the two stages of one-point contact and two-point contact can be modeled and analyzed sequentially.

(2) One-point contact state

Based on the one-point contact stage, then the physical equations and force equations can be established, supplemented by the geometric relationship equations based on the position error as follows:

The physical relationship is:

$$\begin{cases} f=\mu N \\ F_x=k_x(u_0-u) \\ M=-k_s(\theta_0-\theta) \end{cases} \tag{9}$$

The force relationship is:

$$\begin{cases} F_x = N_1 \cos\theta - f_1 \sin\theta \\ F_z = N_1 \sin\theta + f_1 \cos\theta \\ M = F_v(L_p - l + l_1) - F_v \end{cases} \tag{10}$$

Geometric relations for:

$$u - L_p \sin\theta = u_0 - L_p \sin\theta_0 - l_1 - (l - l_1)\tan\theta \tag{11}$$

where l_1 represents the insertion depth during the chamfering contact phase:

$$l_1 = u_0 - l_p \sin\theta_0 + r - R \tag{12}$$

The joint solution yields an expression for the generalized force in the one-point contact phase as:

$$\begin{bmatrix} F_x \\ F_y \\ M \end{bmatrix} = \begin{bmatrix} F_x \\ BF_x \\ F_x(L_p - l + l_1) - F_z r \end{bmatrix} \tag{13}$$

Among them:

$$\begin{cases} B = \dfrac{\sin}{\theta_0} + \mu\cos\theta_0\cos\theta_0 - \mu\sin\theta_0 \\ F_x = \dfrac{k_\circ k_o[(l - l_1)\theta_0 + l_1]}{k_o + k_c(L_\rho - l + l_1)(L_\rho - l + l_1 - Br)} \end{cases} \tag{14}$$

(3) Two-point contact state

In the two-point contact stage, suppose N_1, N_2 is the contact reaction force and f_1, f_2 is the friction force. Considering still only one case, the relevant physical equations, force equations and geometrical relationship equations are as follows:

The physical relationship is:

$$\begin{cases} f_1 = \mu N_1 \quad f_2 = \mu N_2 \\ F_x = k_x(u_0 - u) \\ M = -k_s(\theta_0 - \theta) \end{cases} \tag{15}$$

The force relationship is:

$$\begin{cases} F_x = N_1 \cos\theta - N_2 - f_1 \sin\theta \\ F_z = N_1 \sin\theta + f_2 + f_1 \cos\theta \\ M = F_x(L_p - l + l_1) - F_z r + 2Rf_2 - N_2(l - l_1) \end{cases} \tag{16}$$

Geometric relations for:

$$\begin{cases} (l - l_1)\sin\theta = 2(R - r\cos\theta) \\ u - L_p \sin\theta = u_0 - L_p \sin\theta_0 - l_1 - (l - l_1)\tan\theta \end{cases} \tag{17}$$

The joint solution gives the expression for the generalized force at the two-point contact stage as:

$$\begin{cases} M = \dfrac{2k_s(R - r)}{l - l_1} \\ F_x = k_x\{(L_p - l + l_1)[\theta_0 - \dfrac{2(R - r)}{l - l_1}] + [l_1 + (l - l_1)\theta_0]\} \\ F_z = \dfrac{M \cdot 2\mu + F_x \cdot (2\mu R + l - l_1 - 2L_p)}{2\mu(R - r) - l + L_\kappa} l_1 \end{cases} \tag{18}$$

The insertion depth takes on a range of values:

$$l_2 < l < l_{MAX} \tag{19}$$

Combining the calculation process in the previous section, the expression for the assembly insertion force can be obtained as the following segmented function:

$$F_s = \begin{cases} \dfrac{k_s k_s l}{k_s + k_s L_p (L_p - Ar)} & 0 < l < u_0 - l_p \sin\theta_0 + r - R \\ \dfrac{k_s k_s [(l - l_s)\theta_s + l_1]}{k_s + k_s (L_p - l + l_1)(L_p - l + l_1 - Br)} & u_0 - l_p \sin\theta_0 + r - R < l < l_2 \\ k_s \{(L_p - l + l_1)[\theta_0 - \dfrac{2(R-r)}{l - l_1}] + [l_1 + (l - l_1)\theta_0]\} & l_2 < l < L_{sodx} \end{cases} \tag{20}$$

$$F_s = \begin{cases} \dfrac{\cos\alpha + \mu\sin\alpha}{\sin\alpha - u\cos\alpha} \dfrac{k_s k_s l}{k_s + k_s L_s (L_s - Ar)} & 0 < l < u_s - l_s \sin\theta_s + r - R \\ \dfrac{\sin\theta_s + \mu\sin\theta_s}{\cos\theta_s - \mu\sin\theta_s} \dfrac{k_s k_s L_s (L_s - Ar)}{k_s + k_s (L_s - l + l_s)(L_s - l + l_s - Br)} & u_s - l_s \sin\theta_s + r - R < l < l_s \\ \dfrac{1}{2\mu(R-r) - l + l_s} \cdot (\dfrac{2k_s (R-r)}{l - l_s} \cdot 2\mu + k_s [(L_s - l + l_s) & \\ (\theta_s - 2\dfrac{R-r}{l - l_s}) + l_s + (l - l_s)\theta_s] \cdot (2\mu R + l - l_s - 2L_s) & l_2 < l < L_{sodx} \end{cases} \tag{21}$$

The core of the expression is about the five parameters of the expression for:

$$F_x = f_1(k_x, k_0, u_0, \theta_0, L) \tag{22}$$

$$F_z = f_2(k_x, k_0, u_0, \theta_0, L) \tag{23}$$

In the insertion process, the insertion depth L is a variable, and the structural parameter k_x, k_θ and environmental parameter u_0, θ_0 are invariants. We can study the effect of structural parameters and environmental parameters on assembly force based on the control variable method [21].

2.2. Assembly Position Adjustment and Assembly Flow

2.2.1. Positioning during assembly of shaft holes

High-precision assembly industrial robots can complete the assembly task, the key lies in the adjustment of the assembly position. In the assembly process, the industrial robot clamps the workpiece to carry out the assembly work, due to the initial positioning errors, jitter in the movement process, workpiece processing errors, clamping positioning errors and other errors, the industrial robot needs to take the initiative to adjust the assembly posture of the workpiece. In this process, the industrial robot mainly identifies the assembly state through the contact force between the workpieces, and then adjusts the position of the assembly according to the error situation, including the deflection angle and center displacement error. Since the assembly is mounted on the force sensor, and the force data measured by the sensor are all the force of the force measurement platform, so it is necessary to establish the positional relationship between the assembly and the end axis of the industrial robot, and the force measurement platform of the sensor [22].

Since the assembly error of the shaft-hole assembled workpiece is small and the positioning error during the assembly process is limited, the magnitude of each position adjustment is set to be very small, so that each adjustment of the position can be regarded as a differential motion, from which it can be further approximated as a generalized velocity.

The position vector of the robot end-axis coordinate origin O_B in the contact coordinate system $\{J\}$ is:

$${}^J p = \begin{bmatrix} -r\sin\beta & r\cos\beta & l \end{bmatrix}^{\mathrm{T}} \tag{24}$$

where for r is the radius of the assembly, l is the distance from the bottom center of the shaft to

the center of the moving platform, and β is the angle between the line connecting the two coordinate origins and the Y_B axis.

For any 3-dimensional vector $p=\begin{bmatrix} p_x & p_y & p_z \end{bmatrix}^T$, the antisymmetric matrix is:

$$S(p)=\begin{bmatrix} 0 & -p_z & p_y \\ p_z & 0 & -p_x \\ -p_y & p_x & 0 \end{bmatrix} \tag{25}$$

Therefore, the antisymmetric matrix of ${}^{J}p=\begin{bmatrix} -r\sin\beta & r\cos\beta & l \end{bmatrix}^{\mathrm{T}}$ is:

$$S({}^{J}p)=\begin{bmatrix} 0 & -l & r\cos\beta \\ l & 0 & r\sin\beta \\ -r\cos\beta & -r\sin\beta & 0 \end{bmatrix} \tag{26}$$

According to the helix theory, the coordinate transformation of the generalized velocity between the contact coordinate system $\{J\}$ and the robot end-effector coordinate system $\{B\}$ is:

$$\begin{bmatrix} {}^{B}v \\ {}^{B}\omega \end{bmatrix}=\begin{bmatrix} {}^{B}R & -{}^{B}_{J}RS({}^{J}p) \\ 0 & {}^{B}_{J}R \end{bmatrix}\begin{bmatrix} {}^{J}v \\ {}^{J}\omega \end{bmatrix} \tag{27}$$

Since the contact coordinate system $\{J\}$ and the robot end-effector coordinate system $\{B\}$ have the same attitude, the:

$${}^{B}_{J}R=\begin{bmatrix} 1 & 0 & 0 \\ 0 & 1 & 0 \\ 0 & 0 & 1 \end{bmatrix} \tag{28}$$

If the generalized velocity in the contact coordinate system $\{J\}$ is:

$$\begin{bmatrix} J_v \\ J_\omega \end{bmatrix}=\begin{bmatrix} 0 \\ 0 \\ 0 \\ \delta\alpha \\ \delta\beta \\ 0 \end{bmatrix} \tag{29}$$

Then there is:

$$\begin{aligned} \begin{bmatrix} s_v \\ s_\omega \end{bmatrix} &= \begin{bmatrix} 1 & 0 & 0 & 0 & -l & r\cos\beta \\ 0 & 1 & 0 & l & 0 & r\sin\beta \\ 0 & 0 & 1 & -r\cos\beta & -r\sin\beta & 0 \\ 0 & 0 & 0 & 1 & 0 & 0 \\ 0 & 0 & 0 & 0 & 1 & 0 \\ 0 & 0 & 0 & 0 & 0 & 1 \end{bmatrix}\begin{bmatrix} 0 \\ 0 \\ 0 \\ \delta\alpha \\ \delta\beta \\ 0 \end{bmatrix} \\ &= \begin{bmatrix} -l\cdot\delta\beta \\ l\cdot\delta\alpha \\ -r\cos\beta\cdot\delta\alpha-r\cos\beta\cdot\delta\beta\cdot\sin\beta \\ \delta\alpha \\ \delta\beta \\ 0 \end{bmatrix} \end{aligned} \tag{30}$$

In this way, a mapping of the rotation angle in the contact coordinate system $\{J\}$ to the positional

transformation in the robot end axis coordinate system $\{B\}$ is established. In other words, it is realized that the positional adjustment in the contact coordinate system $\{J\}$ is adjusted by the coordinate transformation in the robot end-effector $\{B\}$.

2.2.2. Shaft Bore Assembly Program and Procedure

In order to better realize high-precision shaft hole assembly, this paper proposes a shaft hole assembly strategy system based on a supple assembly mechanism, which adopts the look-move-touch control method, only introducing a passive adaptation assembly method in the final contact assembly stage. Due to the inclusion of a supple mechanism between the end-effector and the robotic arm, the impact can be avoided during the assembly contact, and the compliant deformation can be generated in a rapid and timely manner to compensate for the positional error, avoiding the cumbersome process of hole search adjustment. Figure 2 shows the shaft hole assembly control process, which mainly includes four main steps: searching and positioning, picking up and carrying parts, positioning after clamping, and passive compliant assembly.

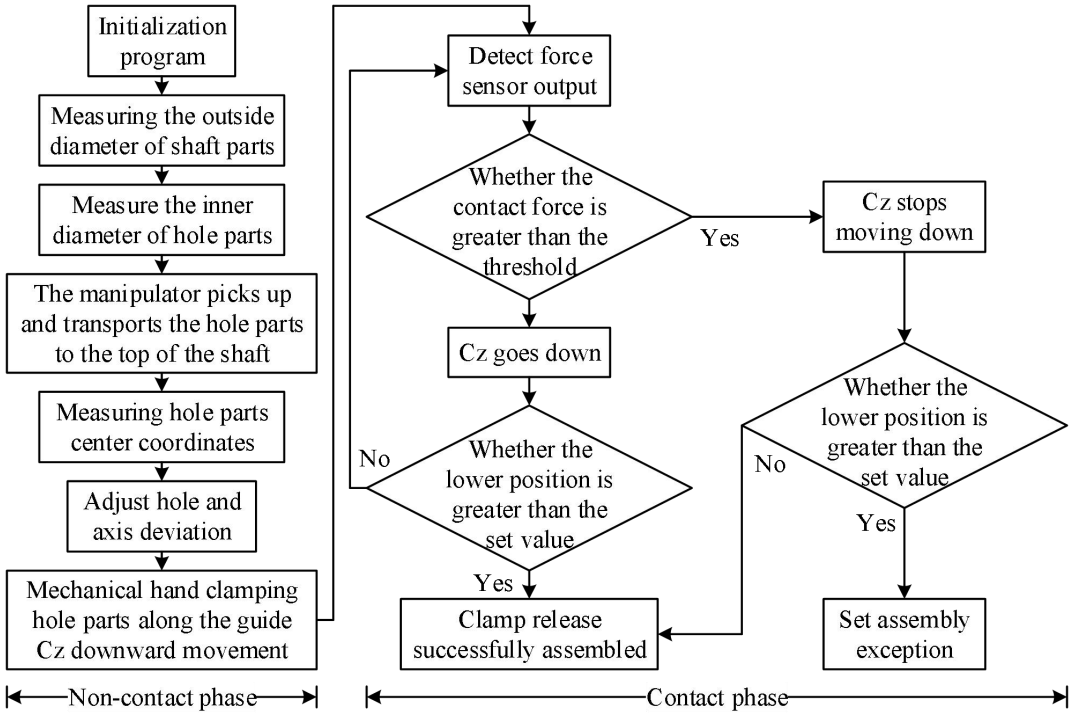

Figure 2. Shaft assembly control process

(1) Search and localization. Through the six-dimensional force sensors to identify the positioning, measured the outer diameter of the shaft as well as the inner diameter of the hole, through the calculation to find the coordinates of the center of the circle. The hole part position is a certain distance away from the shaft part, so it adopts movable machine vision, and the machine vision is mounted on the precision linear guide to realize the movement of two degrees of freedom.

(2) Pick up and carry parts. After localization by the search, search for the target position, guide the robot to clamp the parts to be installed to the target position.

(3) Positioning after clamping. After the hole part is clamped and carried to the top of the shaft, the position changes, so the center of the hole part needs to be re-detected and re-calculated. Through analysis and comparison, the relative positions of the hole and shaft are adjusted so that their center axes coincide with each other, in order to reduce the initial position deviation before assembly contact.

(4) Passive soft assembly. After repositioning, the position error of the hole shaft will be smaller, but due to the influence of the movement error of the motion platform, visual error, installation error of the shaft parts and other factors, the axes of the hole shaft parts cannot be completely coincident, and there will always be a certain amount of lateral deviation and angular deviation. During assembly operations, even small deviations can generate large interaction forces. In order to avoid damage to the parts or equipment and jamming during assembly, the softening mechanism connected between the

robot arm and the gripper finger produces softening deformation to compensate for the positional deviation in order to complete the assembly.

3. Flexible assembly system construction

Industrial robot is a product of the information age, integrated with information technology, communication technology and other modern technologies, making industrial production, communication and control has a higher level of intelligence, improve overall production efficiency, expand production capacity, but also accelerate the pace of development of industrial modernization. At this stage, with the expansion of the scale of industrial production, industrial robots have become an important production element of some large-scale industrial enterprises, to assume part of the manual work, reducing the artificial input, transforming the mode of production, and promoting industrial modernization.

3.1. General structure of the flexible assembly system

3.1.1. Assembly Robot Flexibility Control Principles

The design of the flexure control system mainly needs to solve two problems, one is how to interface with the passive flexure process, and the other is how to complete the assembly task in the hole entry stage. Based on the consideration of the uncertainty of the environmental factors, this paper will use the force ring, inclusive position ring of the inner and outer ring serial control method, when the shaft hole does not contact, the assembly continues to be assembled under the position servo system of the inner ring, and when the shaft hole contact occurs, the outer ring will be triggered, and the position adjustment signal will be calculated by the outer ring according to the collision force. And since the inner ring has a certain position servo stiffness, the uncertainty of the outer ring's recognition of the environment will be compensated by the strong robustness of the inner ring [23].

In a mass-spring damped system, a certain displacement x occurs when the system is subjected to a force F, and the displacement is related to the force:

$$F = m\ddot{x} + c\dot{x} + kx \tag{31}$$

The mass-spring damping system can establish the relationship between force and displacement, and through the parameter configuration of m,k,c, the system can be made to produce the ideal amount of position adjustment when the force is applied, so in the assembly active suppleness control, the relationship between the contact force and the position adjustment can be established by the suitable mass-spring damping system.

First assume the environment stiffness is a constant value K, then the force relationship between the environment and the virtual system at this time is given by:

$$F = Kx_e = m\ddot{x} + c\dot{x} + k(x - x_e) \tag{32}$$

If the quasi-static model is considered, the velocity and acceleration terms of the mechanism are neglected, so the relationship between collision depth x_s and displacement x can be derived as:

$$x_e = \frac{k}{K + k}x \tag{33}$$

And in the actual system $K \gg k$, so the collision depth is a very small value, so in the stability analysis can be ignored in the collision depth, the collision process is equivalent to the collision force generated only at the time of contact, simplified to obtain the transfer function of the system block diagram shown in Figure 3.

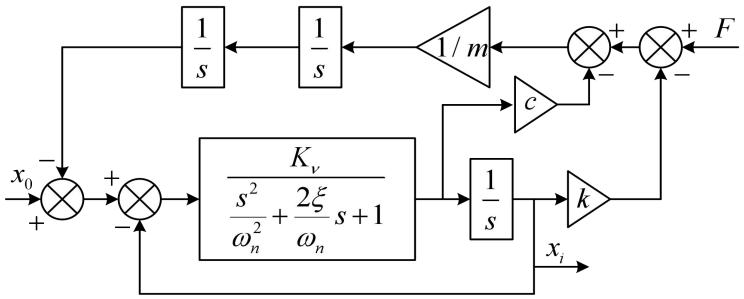

Figure 3. Transfer function square diagram

As can be seen from the block diagram of the transfer function of the system, the inner loop of the system is still the position loop, and the force in the outer loop does not appear as a feedback signal, but rather in the dynamics loop with through the solution of the virtual model, which produces the corresponding position adjustment amount. Based on the above figure, the open-loop transfer function of the system is given as:

$$G_{kx}(s)=\frac{K_v cs+K_v k}{ms^2\left[s\left(\frac{s^2}{\omega_n^2}+\frac{2\xi}{\omega_n}s+1\right)+K_v\right]} \tag{34}$$

Its closed-loop transfer function is:

$$G_{kx}(s)=\frac{K_v}{ms^2\left[s\left(\frac{s^2}{\omega_n^2}+\frac{2\xi}{\omega_n}s+1\right)+K_v\right]+K_v cs+K_v k} \tag{35}$$

Where c is the virtual damping of the system, m is the virtual mass of the system and k is the virtual stiffness of the system.

For the above equation can be based on its system closed-loop characteristic equation by Routh criterion, the stability condition of the active flexible control system is given as:

$$\begin{cases} 0<K_v<2\xi\omega_n \\ \dfrac{k}{c}<K_v \\ m>\dfrac{2\xi}{\omega_n}\dfrac{2\xi\omega_n c-k}{2\xi\omega_n-K_v} \\ m>\dfrac{K_v(2\xi\omega_n c-k)^2}{(K_v c-k)\omega_n^2(2\xi\omega_n-K_v)} \end{cases} \tag{36}$$

In the stability conditions, the first condition is the same as the position control system stability condition, which indirectly shows that the precondition for the stability of the force loop inclusive position loop control method is that the position loop must be stable. The second stability condition shows that the virtual damping and virtual stiffness need to satisfy the parameter condition that the ratio of virtual stiffness to virtual damping cannot be greater than the open-loop gain of the position system. The third and fourth stability conditions show the conditions that need to be satisfied for the virtual mass, which are relatively easy to satisfy.

3.1.2. Flexible assembly systems for assembly robots

Based on the comprehensive analysis of the previous paper, as the force sensing part of the flexible assembly system, this paper selects the integral preloaded parallel six-dimensional force sensor, which has the characteristics of high precision, small stress coupling, no over-zero, no hysteresis and so on. And the actuator is chosen to be 6-PUS/UPS parallel robot, which has the advantages of large stiffness-to-weight ratio, simple structure, low moving mass, good dynamic performance and large working space. In addition, the flexible assembly system also includes an industrial computer with Windows XP operating system, data acquisition related components, etc..

The logical structure of the flexible assembly system is shown in Figure 4. The working principle of

the flexible assembly system is to correct the relative position and movement of the assemblies through the contact force detected by the force sensing system equipped with it, and the flexible assembly system can actively adjust the relative position between the shaft parts and the holes to comply with and eliminate the assembly errors, and finally realize the assembly task.

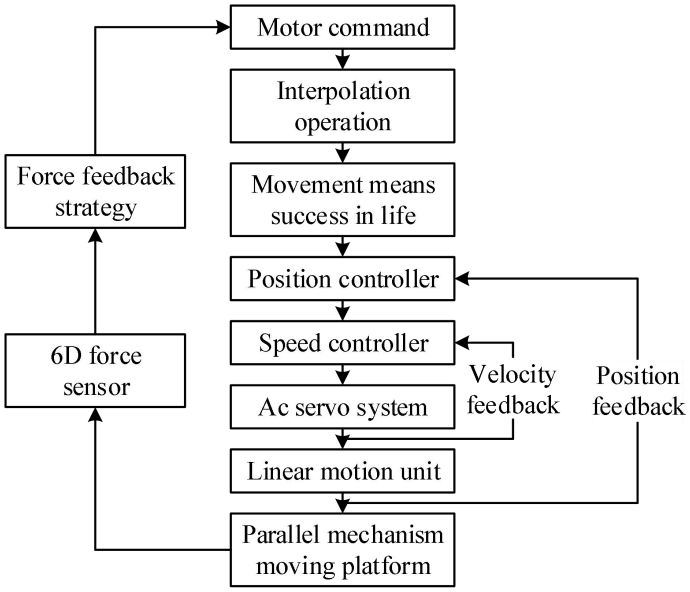

Figure 4. The logical structure of the flexible assembly system

After the parallel robot receives the motion command, it carries out interpolation, inverse solution and other operations, then generates the motion file, drives the linear motion unit through the controller and AC servo system, and finally controls the parallel robot moving platform to move at a certain speed. When the robot moves to a certain position and is about to contact with the external environment, the force sensing system starts to detect the force at the end of the parallel robot moving platform in real time, once there is contact force, the flexible assembly control system will convert the contact force information into the position deviation information of the moving platform according to the force feedback strategy. Thus, the corresponding target position of the parallel robot moving platform is calculated, and the above process is repeated to finally realize the adjustment and correction of the position of the end of the moving platform.

3.2. Assembly of industrial robotic actuation systems

3.2.1. Kinematic Inverse Solution for Assembly Robots

The 6PUS-UPU parallel robot is a parallel mechanism based on the Stewart mechanism, consisting of a fixed platform, a moving platform, and a branch connecting the fixed platform and the moving platform. It is characterized by the fact that the fixed platform is connected to the moving platform through six identical drive branches PUS (mobile vice - hoke hinge - ball vice) and one middle branch UPU (hoke hinge - mobile vice - hoke strand) [24].

The kinematic inverse solution of the 6PUS-UPU parallel robot is mainly divided into the position inverse solution of the six PUS branches and the position inverse solution of the middle one UPU branch. For this parallel robot, the fixed coordinate system is established on the center of the circle where the six Hook strands of the PUS branches are located, and the dynamic coordinate system is established on the center of the circle where the six ball pairs are located.

Let the position parameter of the origin of the moving coordinate system in the fixed coordinate system be $({}^{A}P_{X}\ {}^{A}P_{Y}\ {}^{A}P_{Z})$, then the coordinates of the moving platform in the fixed coordinate system $({}^{A}P_{X}\quad {}^{A}P_{Y}\quad {}^{A}P_{Z}\quad \alpha\quad \beta\quad \gamma)$ are the parameters that have already been determined, the hinge point on the fixed platform in the fixed coordinate system has a position parameter of $A_i = {}^{4}\left[X_i\quad Y_i\quad Z_i\right]^{T}\ (i=1,2,\cdots,6)$, and the hinge point on the moving platform has a position parameter of $b_i = {}^{B}\left[X_i\quad Y_i\quad Z_i\right]^{T}\ (i=1,2,\cdots,6)$ in the moving coordinate system.

According to the knowledge of robotics, the transformation relationship between the moving coordinate system and the fixed coordinate system is obtained as:

$$ {}^{A}_{B}R(\alpha,\beta,\gamma)=\begin{bmatrix} c\beta c\gamma & -c\beta s\gamma & s\beta \\ s\alpha s\beta c\gamma+c\alpha s\gamma & -s\alpha s\beta s\gamma+c\alpha c\gamma & -s\alpha c\beta \\ -c\alpha s\beta c\gamma+s\alpha s\gamma & c\alpha s\beta s\gamma+s\alpha c\gamma & c\alpha c\beta \end{bmatrix} \tag{37} $$

The coordinates of the more chained points of the moving platform in the fixed coordinate system can be obtained from the transformation relation:

$$ B_i={}^{A}_{B}Rb_i+P \quad (i=1,2,...,6) \tag{38} $$

Where, $P=\begin{bmatrix} {}^{4}P_X & {}^{A}P_Y & {}^{A}P_Z \end{bmatrix}$ the position vector of the origin of the moving coordinate system in the fixed coordinate system.

From the coordinates of the hinge point of the Hooke's strand coordinates and the moving platform coordinates at the drive rod, and then according to the geometric relationship to get the position of the drive slider as:

$$ Z_i=\left[L^2-(A_i(1)-B_i(1))^2-(A_i(2)-B_i(2))^2\right]^{1/2}+B_i(3) \tag{39} $$

Where $i=1,2,...6$, $A_i(1),A_i(2)$ for the fixed platform hinge point in the fixed coordinate system under the X coordinates and Y coordinates. $B_i(1),B_i(2)$ is the X,Y coordinate of the hinge point of the moving platform in the fixed coordinate system. L is the length of the linkage between the hinge points of the moving and fixed platforms.

The displacement of the base coordinate system $o-x_oy_oz_o$ of the intermediate branch with respect to the fixed coordinate system $\{A\}O-X_oY_oZ_o$ is $(0\quad 0\quad -l_{b_0})$, and the Euler angle $Z-Y-X$ is $(-\pi/_2\ -\pi/_2\ 0)$, thus the transformation relation ${}^{O}_{o}T$ of the intermediate branch coordinate system with respect to the fixed coordinate system can be obtained as follows:

$$ {}^{O}_{o}T=\begin{pmatrix} c\alpha c\beta & c\alpha s\beta s\gamma-s\alpha c\gamma & c\alpha s\beta c\gamma+s\alpha s\gamma & 0 \\ s\alpha c\beta & s\alpha s\beta s\gamma+c\alpha c\gamma & s\alpha s\beta c\gamma-c\alpha s\gamma & 0 \\ -s\beta & c\beta s\gamma & c\beta c\gamma & -l_{s_0} \\ 0 & 0 & 0 & 1 \end{pmatrix}=\begin{pmatrix} 0 & 1 & 0 & 0 \\ 0 & 0 & 1 & 0 \\ 1 & 0 & 0 & -l_{s_0} \\ 0 & 0 & 0 & 1 \end{pmatrix} \tag{40} $$

The displacement of the moving coordinate system system with respect to the coordinate system $o-x_5y_5z_5$ of the intermediate branch is $(0,l_{m_5},0)$ and $Z-Y-X$ the Euler angle is $(\pi,0,\pi/2)$. From this, we can obtain the transformation relation ${}^{s}_{T}T$ of the coordinate system with respect to the coordinate system $o-x_5y_5z_5$ of the intermediate branch, and at the same time, we can find the transformation relation ${}^{o}_{T}T$ of the moving coordinate system with respect to the fixed coordinate system.

Now θ_1:

Since ${}^{1}_{T}T={}^{1}_{T}T\,{}^{0}_{T}T={}^{O}_{o}T^{-1}({}^{0}_{o}T\,{}^{T}_{o}T)$, and at the same time ${}^{1}_{T}T={}^{1}_{2}T\,{}^{2}_{3}T\,{}^{3}_{4}T\,{}^{4}_{5}T\,{}^{5}_{T}T$, making the two matrices equal, we obtain:

$$ \theta_1=\arctan\left(\frac{l_{m_5}\sin\beta-p_x}{l_{m_5}\cos\alpha\cos\beta-p_x-l_{b_0}}\right) \tag{41} $$

The relationship between γ and the other five parameters $(x\quad y\quad z\quad \alpha\quad \beta)$ at the end can be calculated as:

$$ \gamma=\arctan\left(\frac{\sin a\sin\theta_1}{-\sin\theta_1\cos\alpha\sin\beta-\cos\beta\cos\theta_1}\right) \tag{42} $$

3.2.2. Motion Control Strategy for Assembly Robots

The 6-PUS/UPU parallel robot also has force interactions between the end-effector and the processed objects during the actual machining or assembly process. Due to a combination of factors, it is very easy to generate internal forces during operation, causing mechanical vibration, and thus difficult to ensure the task accuracy.The hybrid force/position control strategy of the 6PUS-UPU parallel robot means that the non-redundant branch adopts position control to determine the position of the moving platform and to ensure the mechanism's operating accuracy. The redundant branch adopts force control to improve the force distribution of each branch and increase the stiffness of the mechanism. Position control and force control work together to improve the motion accuracy of the mechanism.

According to the 6PUS-UPU parallel machine manpower/position hybrid control requirements, it is first necessary to carry out trajectory planning for the moving platform to find out the physical quantities such as position, speed, acceleration, etc. of the moving platform. Through the inverse kinematics calculation of the parallel mechanism, the position control instruction of each non-redundant branch is derived, and the position control is performed for each of the five sub-redundant branches, which ultimately enables the moving platform to complete the planned motion. Through the inverse kinematics calculation of the parallel mechanism, the redundant branch force is derived and optimized, and the force control is carried out on the redundant branch to improve the force of the other driving branches. Through the non-redundant branch position control and redundant branch force control, the operating accuracy of the studied mechanism is improved and the dynamic performance of the system is improved.

3.3. Robot End Mechanical Sensing System

3.3.1. Principles of Robot Mechanical Perception Capability

The force sensing capability of a high-precision assembly industrial robot is a prerequisite for accomplishing force control experiments. Installing a six-dimensional force sensor at the end of an industrial robot that can detect six-dimensional force information in real time, which is constantly changing in size and direction, is able to realize the force perception of the industrial robot. In this experiment, a double-layer pre-tensioned parallel six-dimensional force sensor is used as the force sensing unit, and it is successfully installed at the end of the industrial robot, which is capable of real-time detection of force information.

The whole system is centered on 6-PUS/UPS, equipped with computer, USB isolator, data acquisition card and six-dimensional force sensor. When the system works, firstly, you need to input the specified program commands on the computer, and the computer compiles the commands and sends them to the robot for position control. Then when the robot movement process six-dimensional force sensor on the robot end of the force situation for real-time detection, the detected information for filtering, de-interference, amplification processing. Then through the data bus transmission to the computer, the computer will be these force data integration through the set up control program for feedback control. Thus, the robot carries out position control according to the collected three-dimensional spatial full force information, drives the next movement of the robot, and completes the active supple control.

3.3.2. Data calibration of six-dimensional force sensors

In the use of six-dimensional force sensors for force information collection, you need to calibrate the sensor first. The gravity of the sensor itself and the contact handle mounted on the end of the flange will also affect the sensor's indication, in order to measure the real contact force between the contact handle and the workpiece, on the basis of completing the calibration of the sensor, it is necessary to eliminate the influence of these gravity forces on the sensor in real time, i.e., real-time gravitational compensation of the sensor [25].

After the robot end flange, sensor and contact handle are clamped, each time it is used, it is necessary to calibrate the force offset F_{x0}, F_{y0}, F_{z0} and moment offset T_{x0}, T_{y0}, T_{z0} of the three coordinate axes of the sensor, as well as the magnitude of the gravity force and the gravity force's coordinates in the sensor coordinate system G, X, Y, Z on the spot.

First, the robot's six position points are set when the gravity is located in the positive and negative directions of the X-axis, the positive and negative directions of the Y-axis, and the positive and negative directions of the Z-axis of the sensor. When the robot is at each bit posture point, the force and moment readings of the six dimensional force sensor at that moment are recorded, and after completing one calibration, then the collected data has:

$$data = \begin{bmatrix} F_{x1} & F_{y1} & F_{z1} & T_{x1} & T_{y1} & T_{z1} \\ F_{x2} & F_{y2} & F_{z2} & T_{x2} & T_{y2} & T_{z2} \\ F_{x3} & F_{y3} & F_{z3} & T_{x3} & T_{y3} & T_{z3} \\ F_{x4} & F_{y4} & F_{z4} & T_{x4} & T_{y4} & T_{z4} \\ F_{x5} & F_{y5} & F_{z5} & T_{x5} & T_{y5} & T_{z5} \\ F_{x6} & F_{y6} & F_{z6} & T_{x6} & T_{y6} & T_{z6} \end{bmatrix} \tag{43}$$

The coordinate system of the whole system is right-handed and the moments satisfy the right-handed helix rule.

The gravity of the sensor and the contact handle is fixed in position in the sensor coordinate system. In each attitude, the gravity influence is similar, assuming that the sensor zero-drift value is fixed each time it is energized for use, then the data collected through the above calculations have:

$$\begin{cases} G = \dfrac{|F_{x1} - F_{x2}| + |F_{y3} - F_{y4}| + |F_{z5} - F_{z6}|}{6} \\ F_{x0} = \dfrac{F_{x1} + F_{x2}}{2}, F_{y0} = \dfrac{F_{y3} + F_{y4}}{2}, F_{z0} = \dfrac{F_y}{2} \\ T_{x0} = \dfrac{T_{x3} + T_{x4} + T_{x5} + T_{x6}}{4}, T_{y0} = \dfrac{T_{x1} + T_{x2} + T_{x5} + T_{x6}}{4} \\ T_{z0} = \dfrac{T_{x3} + T_{x4} + T_{x1} + T_{x2}}{4}, X = \dfrac{T_{y6} - T_{y5} + T_{z3} - T_{z4}}{4G} \\ Y = \dfrac{T_{z2} - T_{z1} + T_{x5} - T_{x6}}{4G}, Z = \dfrac{T_{y1} - T_{y2} + T_{x4} - T_{x3}}{4G} \end{cases} \tag{44}$$

When the robot moves, to obtain the true strength of the contact handle in contact with the workpiece, on the basis of the sensor measurement data, it is necessary to add zero drift compensation and gravity compensation, this paper assumes that the installation so that the sensor coordinate system and the robot end coordinate system direction is the same. By writing the robot's six attitude point programs in the teach pendant, let the robot move to the point in sequence, write the above calibration and compensation method into a module and integrate it into the CodeSys platform, when the host computer is connected to the robot, it will run the trajectory program of the teach pendant calibration and compensation, and carry out the sensor calibration and compensation.

4. Flexible control strategies for assembly industrial robots

With the efficient development of various types of technology, the application of industrial robots in the industrial field has been very common, and its importance to the national economic construction is self-evident. The application of industrial robots in the field of automation has greatly improved the overall level of industrial automation, and the development prospect is very broad. Although some of the technology is not yet fully mature, but has laid a stable foundation for the construction of industrial intelligence. Industrial robots are no longer unfamiliar to most people, and all kinds of service-oriented technologies born from robotics have been integrated into people's daily lives. This shows that further enhancement of high-precision assembly of industrial robots with automatic control and servo control optimization is very practical significance.

4.1. Variational method and impedance control principle

4.1.1. Mathematical expression of the variational approach

The calculus of variations is a field of mathematics dealing with functions that ultimately seeks extreme value functions that allow the generalized function to take on extremely large or small values. The key theorem of the variational method is the Euler-I-Lagrange equation, which corresponds to the critical point of the generalized function.

Let $J[y(x)]$ be a generalized function defined on the set of functions $F = \{y(x)\}$, $y(x)$ become the metric of $J[y(x)]$, and F be the domain of definition of $J[y(x)]$. For any fixed value $x \in [x_0, x_1]$, the difference $y(x) - y_0(x)$ between a function $y(x)$ and another desirable function

$y_0(x)$ is called the variation of the function $y(x)$ at $y_0(x)$, denoted:

$$\delta y = \varepsilon y(x) = y(x) - y_0(x) \tag{45}$$

Let $F = (x, y(x), y'(x))$ be a known function of three independent variables $x, y(x), y'(x)$ on an interval $x \in [x_0, x_1]$ with second-order continuous differentiability, $\eta(x)$ be an arbitrary function, and ε be a small parameter, then the increment of $F = (x, y(x), y'(x))$ is:

$$\Delta F = F(x, y(x) + \varepsilon\eta, y'(x) + \varepsilon\eta') - F(x, y(x), y'(x)) \tag{46}$$

This can be obtained by the Taylor median theorem for binary functions:

$$\Delta F = \frac{\partial F}{\partial y}\varepsilon\eta + \frac{\partial F}{\partial y'}\varepsilon\eta' + R_1 \tag{47}$$

where R_1 is a higher order infinitesimal for $\varepsilon \to 0$, then:

$$\delta F = \frac{\partial F}{\partial y}\varepsilon\eta + \frac{\partial F}{\partial y'}\varepsilon\eta \tag{48}$$

It is called the variation of the generalized function $F = (x, y(x), y'(x))$ over $y(x)$, also known as the variation of the generalized function.

Let the function $\Phi(x) \in C[x_0, x_1]$ be continuous and for any function $\eta(x) \in C^1[x_0, x_1]$ continuous and satisfying $\eta(x_0) = \eta(x_1) = 0$, always makes the integral:

$$\int_{x_0}^{x_1} \Phi(x)\eta(x)dx = 0 \tag{49}$$

Holds, then in the interval $[x_0, x_1]$ must be $\Phi(x) \equiv 0$.

Let function $\Phi(x)$ be continuous in the closed plane region D any function $\eta(x, y)$ and its first-order inverse are continuous in the region D and satisfy $\eta(x, y) = 0$ on the boundary line Γ of D, always making the integral:

$$\iint_D \Phi(x, y)\eta(x, y)dxdy = 0 \tag{50}$$

Holds, then there must be $\Phi(x, y) \equiv 0$ on region D.

4.1.2. Mathematical principles of impedance control

For the robotic arm system, the control principle is to control the position of the robotic arm and the dynamic relationship between the contact force of the robotic arm and the outside world by adjusting the impedance parameter after the contact between the robotic arm and the environment, so as to realize the control of force and position. When the end tool of the robotic arm is in contact with the external environment, it is no longer a separate entity, but coupled with the external environment. Mathematical modeling analysis of the ideal spring damping model, you can use the second-order differential equation to express the mathematical model in the following form:

$$\begin{cases} M_d\ddot{X} + B_d\dot{X} + K_d(X - X_d) = -F \\ M_d\ddot{X} + B_d(\dot{X} - \dot{X}_d) + K_d(X - X_d) = -F \\ M_d(\ddot{X} - \ddot{X}_d) + B_d(\dot{X} - \dot{X}_d) + K_d(X - X_d) = -F \end{cases} \tag{51}$$

Where M_d is the desired inertia matrix, B_d is the desired damping matrix, K_d is the desired stiffness matrix, X_d is the desired kinematic position, x is the actual kinematic position, and F is the contact force. $\dot{X}, \ddot{X}$ is the actual velocity and actual acceleration, $\dot{X}_d, \ddot{X}_d$ is the desired velocity and desired acceleration.

Let F_d be the desired contact force, F_e be the actual contact force, and introduce the force deviation E_f into the impedance model, and adopt the third impedance representation model, then the model equation is expressed as:

$$M_d(\ddot{X}-\ddot{X}_d)+B_d(\dot{X}-\dot{X}_d)+K_d(X-X_d)=e_f \tag{52}$$

The above equation is Lagrange transformed to obtain the desired impedance equation as:

$$H(s)=\frac{E(s)}{E_f(s)}=\frac{1}{M_d s^2+B_d s+K_d} \tag{53}$$

Where $E(s)$ is the difference between the desired position and the actual position of the robot arm, the desired position is obtained from the teaching mode, and the actual position is solved by the feedback of the robot arm encoder.

4.2. Robot Flexibility Control Strategy Design

4.2.1. Linearization based on variational methods

In order to meet the real-time demand for motion control of high-precision assembly industrial robots, linearization of the nonlinear dynamics model is needed to simplify the controller design and solution process. The linearization of a nonlinear system is a local approximate description of the system around a reference trajectory, and the closer the points are to the reference trajectory region, the higher the accuracy of its linearization. Based on this, this paper introduces the variational method to linearize the industrial robot motion model. Variational-based linearization is realized by means of the differential form of the reference action path, which can be roughly considered as a linear approximation of the distance between two points on a nonlinear manifold.

The different families of paths $R^{\wedge}$ of an industrial robot can be represented by an exponential mapping as:

$$\begin{aligned} R^{\text{解}}(t) &= R(t)\exp^{{}^{B}\hat{\eta}(t)} \\ R(t) &\in SO(3) \\ {}^{B}\hat{\eta}(t) &\in so(3) \end{aligned} \tag{54}$$

where ${}^{B}\hat{\eta}(t)$ denotes the antisymmetric matrix of rotation angles and $\exp(\cdot)$ is the exponential mapping $so(3)\to SO(3)$, which can be expressed as:

$$e^{\hat{\eta}}=\sum_{k=0}^{\infty}\frac{t^k}{k!}\hat{\eta}^k \tag{55}$$

The infinitesimal variation with respect to the reference trajectory $R_d(t)\in SO(3)$ of the industrial robot can be defined as:

$$\delta R(t)=\frac{d}{d\varepsilon}\Big|_{\varepsilon=0} R_d(t)\exp(\varepsilon\,{}^{B}\hat{\eta})=R_d(t)\,{}^{B}\hat{\eta} \tag{56}$$

The variation of the angular velocity of the corresponding object is divided into:

$$\delta\,{}^{B}\omega(t)={}^{B}\hat{\omega}^{d}(t)\,{}^{B}\eta(t)+{}^{B}\dot{\eta}(t) \tag{57}$$

where ${}^{B}\hat{\omega}^{d}(t)$ denotes the desired angular velocity represented by the dynamic coordinate system.

If the actual rotation matrix $R(t)$ and the desired rotation matrix $R_d(t)$ are close enough, $\delta R(t)$ and $\delta^{B}\omega(t)$ can be considered as a linear approximation of the error of the system between $SO(3)$ the desired state and the actual state, and the error between the two states is denoted as:

$$\begin{cases} e_R(t)=\dfrac{1}{2}(R_d^T(t)R(t)-R^T(t)R_d(t))^{\vee} \\ e_\omega(t)={}^{B}\omega(t)-(R^T(t)R_d(t))\,{}^{B}\omega_d(t) \end{cases} \tag{58}$$

where the superscript symbol $(\cdot)^{\vee}$ denotes mapping $\vee: so(3)\to\mathbb{R}^3$.

4.2.2. Flexible control strategies for industrial robots

The main difficulty in controlling the assembly task of industrial robots by impedance control

strategy alone is the inability to obtain accurate knowledge of the environment. Based on this, this paper constructs an adaptive impedance control strategy based on the industrial robot motion model linearized by the variational method and combined with impedance control to ensure the automatic control and servo control system optimization of high-precision assembly industrial robots.

According to the model reference adaptive control method, an ideal impedance model is set for the adjustable parametric impedance control system, and the adjustment methods of parameters $p(t), q(t)$ and $r(t)$ are analyzed according to the Lyapunov stability principle, so that the actual response of the adjustable parametric impedance control system follows the response of the ideal reference model. The following second-order system is taken as the ideal reference model:

$$\ddot{e}_m + p_m \dot{e}_m + q_m e_m = 0 \tag{59}$$

The ideal reference model of the second-order system is transformed into the following state-space form:

$$\dot{E}_m = \begin{bmatrix} 0 & 1 \\ -q_m & -p_m \end{bmatrix} E_m = A_m E_m \tag{60}$$

where $E_m = [e_m, \dot{e}_m]^T$.

Then the error equation between the actual response of the system and the ideal reference response is:

$$\dot{E}_w = A_m E_w + l(A_m - A(t)r)E - [0, r(t)]^T \tag{61}$$

$$\dot{E}_w = \begin{bmatrix} 0 & 1 \\ -q_m & -p_m \end{bmatrix} E_w + \begin{bmatrix} 0 & 0 \\ q(t)-q_m & p(t)-p_m \end{bmatrix} + \begin{bmatrix} 0 \\ -r(t) \end{bmatrix} \tag{62}$$

Eq. $E_w = [(e_m - e), (\dot{e}_m - \dot{e})]^T$, construct the following Lyapunov function:

$$V = \frac{1}{2} E_w^T R E_w + \frac{1}{2} a_1 (q - b_m)^2 + \frac{1}{2} a_2 (p - a_m)^2 + \frac{1}{2} a_3 r^2 \tag{63}$$

where $R = \begin{bmatrix} s_1 & s_2 \\ s_2 & s_3 \end{bmatrix}$, R, Q are noN·singular symmetric positive definite matrices, $Q = -(A_m^T R + R A_m)$, a_1, a_2 and a_3 are positive constants, $V \geq 0$ (if and only if each of them is 0, $V = 0$), and the derivation of the function V is obtained:

$$\begin{aligned} \dot{V} = &-\frac{1}{2} E_w^T Q E_w + (q - q_m)(ye + a_1 \dot{q}) \\ &+ (p - p_m)(y\dot{e} + a_2 \dot{p}) + g(a_3 \dot{r} - y) \end{aligned} \tag{64}$$

where $y = s_2(e_m - e) + s_3(e_m - \dot{e})$, in an ideal reference system, is taken as $e_m = 0, \dot{e}_m = 0$. To make $\dot{V} < 0$, it is sufficient to satisfy the following relation:

$$\dot{p} = -\frac{y}{a_2}\dot{e}, \dot{q} = -\frac{y}{a_1}e, \dot{r} = \frac{y}{a_3} \tag{65}$$

The above equation is the adjustment method of parameters $p(t), q(t)$ and $r(t)$, the difference between parameters $f(t), g(t)$ and $h(t)$ and $p(t), q(t)$ and $r(t)$ is a constant value, so parameters $f(t), g(t)$ and $h(t)$ and parameters $p(t), q(t)$ and $r(t)$ have the same adjustment law, and in practice, because the real-time measurement of the force signal usually contains a large amount of noise, you can use the speed of the robotic arm instead of the amount of change in the contact force, the adaptive impedance control algorithm is:

$$\begin{cases} h(t) = h(t_0) + a_1 \int_{t_0}^{t} y(t)dt \\ g(t) = g(t_0) - a_2 \int_{t_0}^{t} y(t)e(t)dt \\ f(t) = f(t_0) + a_3 \int_{t_0}^{t} y(t)x(t)dt \\ y(t) = \alpha_d x(t) - \alpha_p e(t) \\ \delta x_r(t) = h(t) + g(t)e(t) - f(t)x(t) \\ x_r(t) = x_r(t_0) + \delta x_r(t) \end{cases} \tag{66}$$

where $a_1, a_2, a_3, \alpha_d, \alpha_p$ are small positive numbers. The model-referenced adaptive control algorithm is used in the design of the impedance controller, which can make the system have better stability and still reduce the trajectory tracking error and force tracking error when accurate environmental information cannot be obtained.

5. Flexibility control validation for assembly industrial robots

In the context of the accelerating process of industrialization, all areas of society are increasing their attention to advanced science and technology in the development of the industrial field, and the emergence of industrial robots has greatly improved the efficiency of industrial production, and thus has been commonly used in the field of automation control. Robots in the industrial field have a high degree of freedom, and as an important part of industrial production equipment, industrial robots have a strong control ability, and are able to carry out automated production based on specific programs, commands issued by humans, and established operating rules. Combined with the irreplaceable value and role of industrial robot technology, high-precision assembly of industrial robots, automatic control and servo control technology also needs to keep pace with the times, to ensure that the level of industrial production to further enhance the lay a solid foundation.

5.1. Gravity Compensation and Impedance Parameter Verification

5.1.1. Validation of Sensor Gravity Compensation

In this paper, when optimizing the automatic control and servo control system of high-precision assembly industrial robots, the flexible control technology is introduced, which uses six-dimensional force sensors for data acquisition and introduces a neutral compensation method to prevent the occurrence of matrix irreversibility due to the repetition of angles in the robot's attitude transformation. In order to better evaluate the accuracy of the algorithm, four counterweights, which are accurately positioned with the mechanical mounting of the sensors, are used for experimental verification. Starting from no load, the counterweight blocks were added gradually, with a total of six scenarios. The gravity of the six-dimensional force sensor's strain housing was obtained at no load, and the sensors acquired the same attitude for all square counterweight scenarios. The sampling frequency of the sensor is adjusted to the highest value for each experiment, and after 500 groups of data are collected continuously, the average value is used as the reference data for each group of experiments.The results of the load parameters of the 6 groups of experiments are shown in Table 1, and the zero point values of the sensors under the 6 kinds of loads are calculated as shown in Table 2.

Table 1. Load gravity and robot installation Angle

Weight quantity	G(N)	x(mm)	y(mm)	z(mm)	θ1	θ2
0	4.69	-1.65	1.12	0.51	-0.56	-0.38
1	17.53	0.08	0.07	-0.63	0.34	-0.32
2	36.82	-0.11	0.16	-1.67	-0.15	-0.26
3	47.61	0.13	-2.75	-2.75	0.18	-0.38
4	58.37	0.09	-0.12	-2.56	0.09	-0.24
5	66.74	0.07	-0.09	-2.42	0.08	-0.22

Table 2. Six-dimensional force sensor zero calculation results

Weight quantity	F_{x0}(N)	F_{y0}(N)	F_{z0}(N)	M_{x0}(N·m)	M_{y0}(N·m)	M_{z0}(N·m)
0	-0.88	0.72	3.98	20.42	32.06	130.61
1	-1.31	-0.49	73.06	43.26	53.18	73.42
2	-2.36	-0.72	69.51	28.17	80.34	78.94
3	-4.83	-1.61	30.15	-44.36	136.59	143.57
4	-5.35	-0.73	54.32	66.45	121.47	146.26
5	-6.04	-0.54	61.47	60.59	124.72	148.85

Because the load gravity is perpendicular to the Z-axis of the robot's tool coordinates when the robot is in a special attitude (A:0◦, B:90◦, C:0◦), the perception error is calculated at this time without the influence of external forces. Using the data in Tables 1 and 2, the gravity error is compensated, and if the error still exists at this point, it is called compensated error. Through the use of calibration accuracy of 0.1g/kg electronic balance weighing, that is, the maximum error of 1N, weighing to obtain the gravity value of the five counterweights, and Table 1 calculated load gravity for comparison, the difference that is the load gravity measurement error. Table 3 Statistical results of error calculation of external force perception and load gravity. Where Fe and M_e are the force/moment magnitude of the sensor after gravity compensation, G is the measured load gravity magnitude, M_g is the moment magnitude of the load on the sensor at robot attitude (A:0◦, B:90◦, C:0◦), and e_F and e_M are the external force/moment perception errors.

From the table, it can be seen that after gravity compensation in the six-dimensional force sensor, the error of perceived external force is within 0.63% of the load, and the error of perceived external moment is within 0.89% of the load-to-sensor moment. And the maximum error of loaded gravity measurement is only 0.31N, which is similar to the maximum error value of electronic balance. Therefore, for the data errors of force and moment, both are significantly lower than the precision deviation of 0.5% for the localization of high-precision assembly industrial robots, which can be explained by the attitude error of industrial robots to fully ensure the assembly precision of industrial robots.

Table 3. The error calculation of external perception and load gravity

External perceptual error calculation						
Weight quantity	F_e(N)	G(N)	e_F (%)	M_e(N·m)	M_g(N·m)	e_M (%)
0	0.031	4.69	0.63	0.008	0.69	0.89
1	0.084	17.53	0.51	0.025	2.64	0.85
2	0.088	36.82	0.35	0.059	6.85	0.82
3	0.112	47.61	0.26	0.078	9.41	0.78
4	0.106	58.37	0.21	0.082	12.38	0.71
5	0.115	66.74	0.17	0.093	14.05	0.63
Load gravity measurement error						
Weight quantity	Calculated value		Measured value		Error value	
0	4.69		4.84		-0.14	
1	17.53		17.79		-0.26	
2	36.82		36.51		0.31	
3	47.61		47.38		0.23	
4	58.37		58.26		0.11	
5	66.74		66.93		-0.19	

5.1.2. Performance effects of impedance parameters

In order to realize force control at the end of a robotic arm, impedance parameters need to be accurately determined, and the choice of parameters directly affects the rate of convergence of the actual force to the desired force. In this section, the relationship between impedance parameters and control performance is explored through a simulation example in which contact is made and a constant contact force is maintained in a one-dimensional direction. The impedance control in one direction will be affected by the inertia parameter, damping parameter and stiffness parameter, for which three different experiments are set up in this paper. Specifically as follows:

(1) Fix the damping parameter and stiffness parameter as 15N·s/mm and 120N/mm, respectively, to verify the positional offset trend of the industrial robot under different inertia parameters, and the specific results are shown in Fig. 5. From the curve in the figure, it can be seen that the overshoot of the industrial robot automatic control and servo control system becomes larger with the value of the inertia

parameter, and the response speed of the end-effector becomes slower. When the inertia parameter is 0.5N·s²/mm, the system can be stabilized faster without overshooting and oscillation, and when the inertia parameter is 9.0N·s²/mm, the maximum value of the system positional offset can reach 1.65mm. In addition, as the inertia parameter decreases, the peak value of the force and the steady state value are also reduced accordingly and the response time is is shortened. As the inertia parameter becomes larger, the force also becomes larger, and the robot is position-controlled, so the position offset becomes larger. Conversely, when the inertia parameter becomes smaller, the force becomes smaller and the position offset becomes smaller. The purpose of impedance control is to counteract the excessive contact force generated when the end comes into contact with the environment due to impedance parameters, such as the inertia of the original arm itself, by setting appropriate impedance parameters in place of the arm's own parameters. By adjusting these parameters, it is possible to ensure that the robotic arm accomplishes its task successfully while protecting the arm and its surroundings from damage.

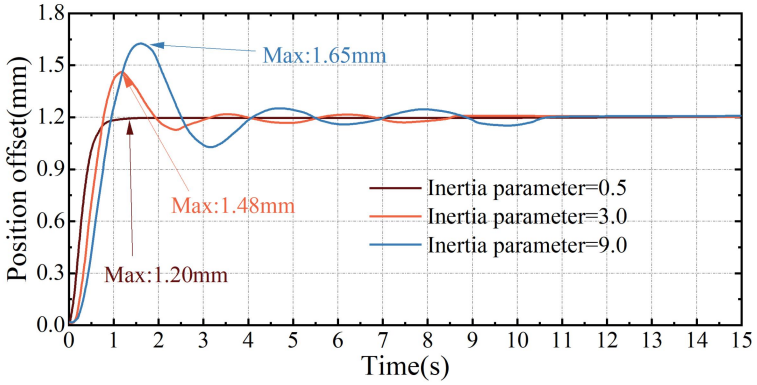

Figure 5. The location offset of different inertial parameters

(2) Fix the inertia parameter and stiffness parameter as 0.5N·s²/mm and 120N/mm, respectively, to verify the change trend of the positional offset of the industrial robot under different damping parameters, and the specific results are shown in Fig. 6. From the curve in the figure, it can be seen that the value of the damping parameter is in a certain small range of the system overshooting amount, when more than this critical value, there is no longer a system overshooting amount. The response speed becomes slower as the value of the damping parameter increases. The system can be stabilized under different damping parameters, but different parameters lead to performance differences. When the damping parameter is 5N·s/mm, the system overshoots more, oscillates more frequently, and takes longer to stabilize. When the damping parameter is 15N·s/mm, the system is in the critical damping state and the stabilization time is short. When the damping parameter is further increased to 25N·s/mm, the system reaches the over-damped state, which can reduce the overshoot but the stabilization time increases significantly and the response speed becomes slower. In the actual high-precision assembly task, the overshoot should be minimized or avoided to prevent the position offset from being too large, affecting the contact force between the shaft and hole parts, which in turn affects the position adjustment in the jacking stage and damages the workpiece or the force sensor. Therefore, the value of the damping parameter should be selected as large as possible within a certain range to minimize the overshoot and shorten the system response time.

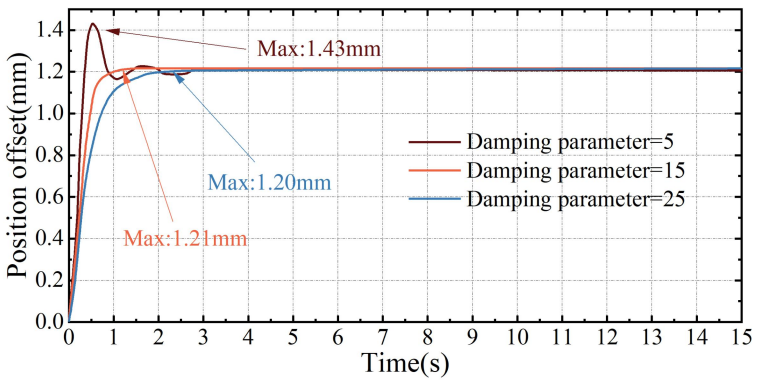

Figure 6. The location offset of different damping parameters

(3) Fix the inertia parameter and damping parameter as 0.5N·s²/mm and 15N·s/mm, respectively, to verify the trend of positional offset of the industrial robot under different stiffness parameters, and the specific results are shown in Fig. 7. The curves in the figure can be seen and the damping parameter of the law of the difference is small, mainly affecting the amount of overshooting of the system. In general, when the stiffness parameter is smaller, the system produces a larger amount of overshoot. When the stiffness parameter in a specific range, greater than a critical value when the system shows the state is no overshooting, but with the increase of the stiffness parameter, the response time will be extended, the response speed becomes slower. When the stiffness parameter exceeds this range, the system overshoots. Therefore, in the process of practical application, the value of the stiffness coefficient should be reduced as much as possible under the premise of ensuring that the system has no overshooting, so as to improve the response speed of the system.

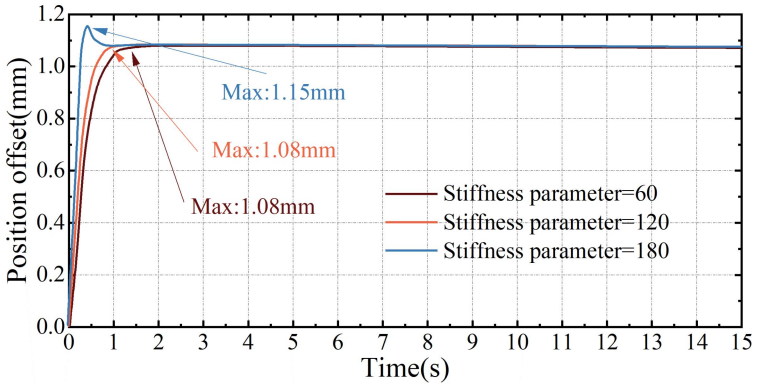

Figure 7. The location offset of different stiffness parameters

5.2. Control experiments for flexible robot assembly

5.2.1. Validation of Flexible Assembly Strategies

In order to verify the effectiveness of the soft assembly strategy proposed in this paper, a simulation experiment platform is built to conduct experiments. The delay time of the response of the whole assembly system is tested to be no more than 25ms, the speed of the robot is set to be 20mm/s in the shaft-hole contact stage, the angular speed of the hole search is set to be 0.4rad/s in the hole search stage, and the radial movement speed of the assembly axis is 5mm/s in the attitude adjustment stage.During the shaft-hole assembly process, the displacement change of the assembly axis is shown in Fig. 8.

From the figure, it can be seen that at 1.48s the assembly axis contacts the outer surface of the hole and enters the shaft-hole contact stage. At 3.00s the assembly shaft is compressed with the flexure device to the set flexure center. At 3.00s to 5.50s the assembly shaft is tilted at an angle of 5.5° along the Y-axis, at 5.50s to 10.00s the assembly shaft is rotated around the Z-axis and enters the stage of searching the hole, at 7.41s a point of contact is made between the assembly shaft and the outer edge of the hole, at 7.41s to 10.00s the assembly shaft is displaced under the elasticity of the elastic displacement device and the displacement is gradually reduced, at At 10.00s, the displacement increases in the reverse direction, and two points of contact occur between the assembly shaft and the outer edge of the hole, at which time the hole searching stage ends.

The assembly axis moves radially toward the center of the assembly hole from 10.00s to 10.82s. At 10.82s, the displacement of the assembly axis changes abruptly and the position adjustment stage of the assembly axis ends. At 10.82s~14.00s, the assembly shaft displacement attitude adjustment stage, the tilt angle gradually decreases, at 10.82s~11.63s, because the friction between the assembly shaft and the hole ratio is greater than the separation of the elastic force of the softening device in the vertical direction, the displacement of the assembly shaft changes less, at 11.63s to 14.00s with the gradual decrease of the tilt angle, its friction force also gradually decreases, the assembly shaft is loaded into the hole under the action of the elastic force, and at the same time the assembly task of the shaft hole is completed.

Between 7.41s and 10.82s, the change value of the flexure center position after the end of the radial movement of the assembly axis is 1.67mm, and when the initial tilt angle is 5.5°, the theoretical change value is 1.72mm, which further verifies the correctness and accuracy of the flexure assembly strategy proposed in this paper.

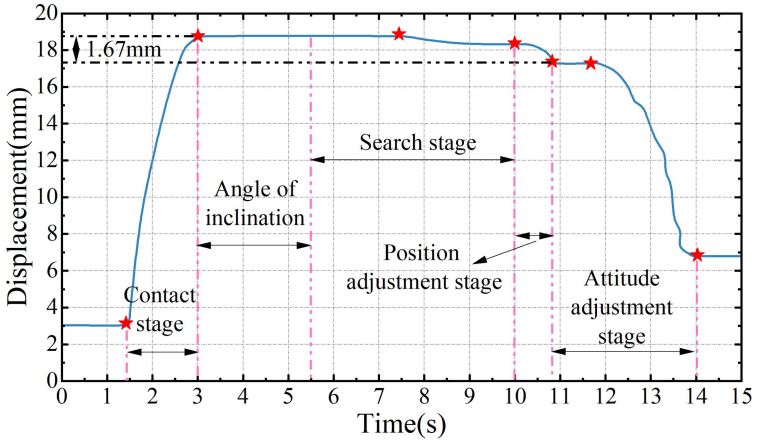

Figure 8. Displacement of the assembly shaft

In order to analyze the shaft hole assembly process more clearly, the tilt angle is set to 5.5°, the angular velocity of the search hole is 0.4 rad/s, the radial moving speed of the assembly shaft position adjustment is 5 mm/s, and the deviation of the shaft hole position is 9 mm. At this time, the trend of the change of the contact force in the process of the assembly of the shaft holes is measured, as shown in Figure 9.

As can be seen from the figure, the contact of the shaft hole occurs at 2.00s to 2.75s, the spring of the flexure device is compressed, and the force in the Z-direction gradually increases. From 2.75s to 4.50s, the tilt angle of the assembly shaft around the Y-axis is 5.5°, due to the assembly shaft and the hole sliding slightly, then the force in the X, Y and Z directions fluctuates, and with the increase of the tilt angle the X-direction force decreases gradually, and the Z-direction force continues to increase, and the Y-direction force does not change much in this process. Between 4.50s~11.00s belongs to the stage of hole searching, the location of the hole is found at 10.00s, at this time the shaft hole is one point of contact, and the hole searching ends at 11.00s, at this time the shaft hole is in the state of two-point contact. Between 11.00 and 12.00, the axial hole appears to move radially, and the force in both X and Z directions decreases gradually. At 12.00~13.75s the inclination angle of the assembly shaft gradually decreases, the assembly shaft is inserted into the assembly hole at this time, and the contact force gradually decreases to 0N.

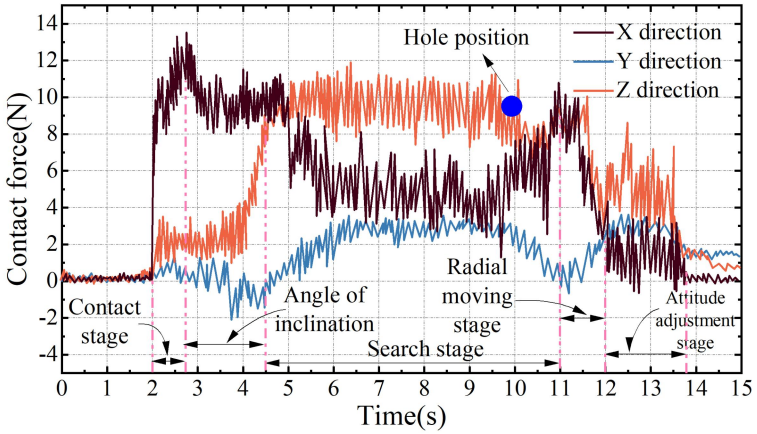

Figure 9. The process of the contact force

5.2.2. Flexible assembly control success rate

In order to further verify the application feasibility of the optimization method of automatic control and servo control system for high-precision assembly industrial robots proposed in this paper, an industrial robot assembly experiment platform was constructed. Twelve groups of aviation plug intergroups were randomly selected to carry out assembly experiments, in which parts A-B, A-C, and A-D are two parts in the aviation plug intergroups, respectively. For the effectiveness of the assembly experiments, this paper chooses coaxiality and parallelism as the evaluation indexes, coaxiality refers to the degree of offset between two axes, and parallelism refers to the degree of offset between two faces. Table 4 shows the experimental results of flexible assembly.

From the table of experimental results, it can be seen that there are some differences in the parallelism of different groups of parts. Taking the first group of data as an example, the parallelism between parts A and B is 4.26 pm, while the parallelism between parts A and C is 8.43 pm, and the parallelism between parts A and D is 7.51 pm. this indicates that there is a large difference in the parallelism between the parts. In addition, there are some differences in the measured values of coaxiality. Again taking the first set of data as an example, the coaxiality between parts A and C is 10.34pm, while the coaxiality between parts A and D is 10.23pm. This indicates that there are some differences in coaxiality between different groups of parts. Assembly time is an important index to measure the assembly efficiency of parts. The experimental results show that the assembly time of different groups of parts fluctuates between 21.65s and 23.42s, and there are some differences. This may be affected by factors such as the shape of parts, structural complexity and assembly difficulty. However, compared with the average time of traditional manual assembly, the system proposed in this paper significantly shortens the assembly time and improves the assembly efficiency.

By analyzing the experimental data in the table in detail, it can be seen that the assembly system proposed in this paper meets the design requirements in terms of key assembly indexes such as assembly success rate, assembly time, parallelism and coaxiality. The high efficiency and stability of the system in the assembly process are verified by the experimental results, which proves the effectiveness and feasibility of the system in industrial production. However, there are some differences between different groups of parts in terms of parallelism, coaxiality and assembly time. This may be due to the differences in manufacturing process, design differences and assembly difficulty of the parts. The variability of parallelism and coaxiality may imply that there are some problems in the quality control of the parts, which need to be more finely controlled and adjusted in the manufacturing process. Therefore, the experimental results provide a more powerful basis for the design and optimization of the automatic control and servo control system of high-precision assembly industrial robots.

Table 4. The results of the flexible assembly

No.	Parallelism(pm)			Coaxial degree(pm)		Assembly time(s)
	A-B	A-C	A-D	A-C	A-D	
1	4.26	8.43	7.51	10.34	10.23	21.65
2	6.59	3.65	4.032	11.15	11.06	22.41
3	5.31	6.53	5.69	8.93	8.98	22.09
4	7.42	10.24	8.35	9.54	9.64	22.17
5	9.54	8.71	4.46	7.92	9.52	23.06
6	10.38	7.75	4.52	8.76	6.57	22.42
7	8.2	5.69	5.97	11.37	7.92	23.18
8	5.69	9.24	8.53	10.22	11.36	23.42
9	9.94	5.65	8.06	9.86	10.53	22.59
10	9.85	5.34	8.17	9.93	10.71	23.04
11	10.12	5.76	5.48	9.42	12.68	22.65
12	9.78	8.41	10.24	6.54	10.59	22.16

5.2.3. Test results for fault-tolerant assembly

In order to further illustrate the assembly reliability of the flexible assembly system designed in this paper with a six-dimensional force sensor, fault-tolerant assembly tests are conducted in this section. In the fault-tolerant assembly test, this paper makes the branch of the sensor faulty by adding simulated fault signals, and the fault monitoring, fault identification, and model reconstruction through the fault-tolerant assembly software, so that the sensor recovers its ability to measure the force, and then the test can be completed successfully. Figure 10 shows the test results of the fault-tolerant assembly, in which Figure 10(a)~(b) shows the reconstructed six-dimensional force and reconstructed six-dimensional moment after adding the fault signal, respectively.

As can be seen from the figures, the fault-tolerant assembly reliability of the automatic and servo control system of the high-precision assembly industrial robot designed in this paper is high, and the force measurement function of the sensors can also be better realized after adding the analog fault signals, which provides support for ensuring the assembly performance of the industrial robot. In addition, in order to show its fault-tolerant ability, we compared normal assembly and fault-tolerant assembly. From the comparison results, when the six-dimensional force sensor is assembled in normal mode and fault-tolerant mode, the adjustment trend is almost the same, and the assembly effect is also very similar, only the size of the adjustment angle has a small difference. For these small differences we can see through the process of many tests, even in the normal assembly mode, after the completion

of the two assembly process, there will be a small difference in the adjustment angle. This is due to the fact that the shaft hole itself and the flange connecting the sensor have a certain degree of flexibility, and the shaft hole has a certain length, so each assembly process will lead to a different state of contact during the spline alignment downstream process. This leads to small differences in the adjustment phase of the assembly process, and it is this uncertainty that proves the correctness and practicality of the algorithm. Therefore, whether under normal or faulty conditions, the optimized industrial robot automatic control and servo control system in this paper can assist the industrial robot to complete the assembly test and achieve the expected results. Thus, the fault-tolerant characteristics of the six-dimensional force sensor have been verified to a certain extent through experiments, which shows that the sensor is able to complete the assembly task under the fault-tolerant mode.

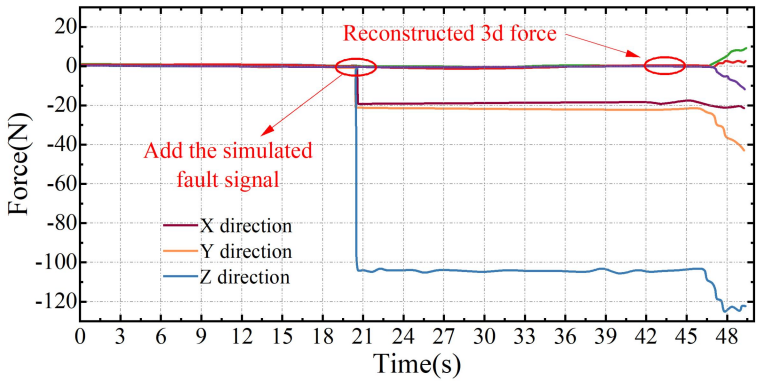

(a) The six dimensions of refactoring

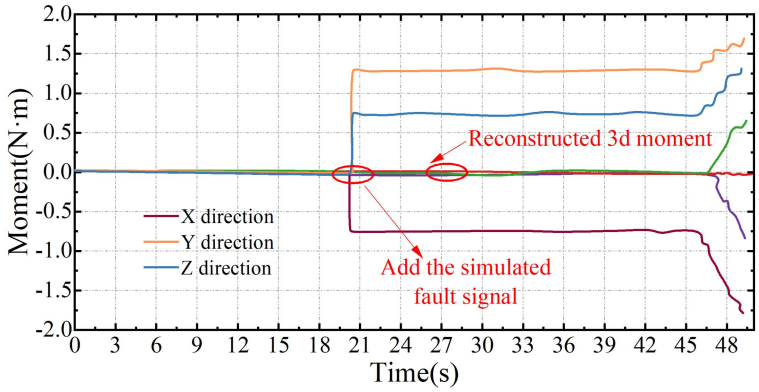

(b) Refactored the six-dimensional moment

Figure 10. Test results of fault tolerant assembly

6. Conclusion

The development of industrial robotics technology makes the manufacturing industry have higher safety, high precision, human-machine interaction and other requirements for the assembly and work of industrial robots, and there is a more urgent need for industrial robots to replace manual labor to complete precision assembly. This paper combines the flexible assembly technology and six-dimensional force sensor optimization of high-precision assembly of industrial robots automatic control and servo control system, and through the variational method of industrial robot motion model linearization, combined with the impedance control design of industrial robots flexible assembly control strategy. Through the control system and optimization strategy designed in this paper, the high-precision shaft hole assembly task is realized, and the optimization of the automatic control and servo control system of high-precision assembly industrial robot based on the variational method is completed.

References

1. Iqbal, J., Islam, R. U., Abbas, S. Z., Khan, A. A., & Ajwad, S. A. (2016). Automating industrial tasks through mechatronic systems-A review of robotics in industrial perspective. Technical Gazette/Tehnički Vjesnik, 23(3).
2. Olszewski, M. (2020). Modern industrial robotics. Pomiary Automatyka Robotyka, 24(1), 5-20.
3. Ma, Y., Xie, Y., Zhu, W., & Liu, S. (2022). An efficient robot precision assembly skill learning framework based on several demonstrations. IEEE Transactions on Automation Science and Engineering, 20(1), 124-136.
4. Peng, Y. C., Jivani, D., Radke, R. J., & Wen, J. (2020, August). Comparing position-and image-based visual servoing for robotic assembly of large structures. In 2020 IEEE 16th International Conference on Automation Science and Engineering (CASE) (pp. 1608-1613). IEEE.
5. Ding, Z., Li, Y., & Zhang, Z. (2020). Electric hybrid control method of assembly line robot based on PLC. Thermal Science, 24(3 Part A), 1505-1511.
6. Lee, J. D., Li, W. C., Shen, J. H., & Chuang, C. W. (2018, April). Multi-robotic arms automated production line. In 2018 4th International Conference on Control, Automation and Robotics (ICCAR) (pp. 26-30). IEEE.
7. Huang, S., Bergström, N., Yamakawa, Y., Senoo, T., & Ishikawa, M. (2016). Applying high-speed vision sensing to an industrial robot for high-performance position regulation under uncertainties. Sensors, 16(8), 1195.
8. Ionescu, D., Filipescu, A., Simion, G., Mincă, E., Cernega, D., Șolea, R., & Filipescu, A. (2022). Communication and control of an assembly, disassembly and repair flexible manufacturing technology on a mechatronics line assisted by an autonomous robotic system. Inventions, 7(2), 43.
9. Ma, Y., Liu, X., Zhang, J., Xu, D., Zhang, D., & Wu, W. (2020). Robotic grasping and alignment for small size components assembly based on visual servoing. The International Journal of Advanced Manufacturing Technology, 106, 4827-4843.
10. Jiang, Y., Huang, X., & Li, S. (2016). An on-line compensation method of a metrology-integrated robot system for high-precision assembly. Industrial Robot: An International Journal, 43(6), 647-656.
11. Tang, S., Liu, G., Lin, Z., & Li, X. (2022). Multi-station test scheduling optimization method for industrial robot servo system. Journal of Ambient Intelligence and Humanized Computing, 1-17.
12. Ma, Y., Du, K., Zhou, D., Zhang, J., Liu, X., & Xu, D. (2019). Automatic precision robot assembly system with microscopic vision and force sensor. International Journal of Advanced Robotic Systems, 16(3), 1729881419851619.
13. Yan, S., Tao, X., & Xu, D. (2021). High-precision robotic assembly system using three-dimensional vision. International Journal of Advanced Robotic Systems, 18(3), 17298814211027029.
14. D'Avella, S., Avizzano, C. A., & Tripicchio, P. (2023). ROS-Industrial based robotic cell for Industry 4.0: Eye-in-hand stereo camera and visual servoing for flexible, fast, and accurate picking and hooking in the production line. Robotics and Computer-Integrated Manufacturing, 80, 102453.
15. Erdős, G., Horváth, D., & Horváth, G. (2021). Visual servo guided cyber-physical robotic assembly cell. IFAC-PapersOnLine, 54(1), 595-600.
16. Zhang, H., Li, M., Ma, S., Jiang, H., & Wang, H. (2021). Recent advances on robot visual servo control methods. Recent patents on mechanical engineering, 14(3), 298-312.
17. Luo, Y., Li, S., & Li, D. (2020). Intelligent perception system of robot visual servo for complex industrial environment. Sensors, 20(24), 7121.
18. Chen, H., Xu, J., Zhang, B., & Fuhlbrigge, T. (2017). Improved parameter optimization method for complex assembly process in robotic manufacturing. Industrial Robot: An International Journal, 44(1), 21-27.
19. Valente, A., Baraldo, S., & Carpanzano, E. (2017). Smooth trajectory generation for industrial robots performing high precision assembly processes. CIRP Annals, 66(1), 17-20.

20. Jianjun Jiao,Zonggang Li,Guangqing Xia,Jianzhou Xin,Guoping Wang & Yinjuan Chen. (2025). An uncalibrated visual servo control method of manipulator for multiple peg-in-hole assembly based on projective homography. Journal of the Franklin Institute(5),107572-107572.
21. Yujia Zang,Zitong Wang,Mingfeng Pan,Zhixuan Hou,Ziqin Ding & Mingyang Zhao. (2025). Safe peg-in-hole automatic assembly using virtual guiding force: A deep reinforcement learning solution. Robotics and Autonomous Systems104894-104894.
22. Jiawei Zhang,Chengchao Bai,Jifeng Guo,Zhengai Cheng & Ying Chen. (2024). Contact State Recognition for Dual Peg-in-Hole Assembly of Tightly Coupled Dual Manipulator. Electronics(18),3785-3785.
23. Claudio Urrea,Pablo Sari,John Kern & Hugo Torres. (2024). Enhancing Adaptability and Autonomy in Cooperative Selective Compliance Assembly Robot Arm Robots: Implementation of Coordination and Rapidly Exploring Random Tree Algorithms for Safe and Efficient Manipulation Tasks. Applied Sciences(15),6804-6804.
24. Yuan Peikang,Liu Jianbin,Branson David T.,Song Zhibin,Wu Shuai,Dai Jian S. & Kang Rongjie. (2024). Design and control of a compliant robotic actuator with parallel spring-damping transmission. Robotica(4),1113-1133.
25. Lu Liu,Xiaoli Jia,Qingyu Yang,Jinglong Zhang,Liaoliang Ke,Jie Yang & Sritawat Kitipornchai. (2025). Design and application of a new high-performance flexible six-axis force/torque sensor for massage therapy. Measurement116312-116312.